Geol. Mag. **00** (*0*), *2008, pp. 1–13.* © *2008 Cambridge University Press*
doi:10.1017/S0016756808005323 *Printed in the United Kingdom*

Travertine deposits from along the South Tibetan Fault System near Nyalam, Tibet

R. ZENTMYER*, P. M. MYROW† & D. L. NEWELL‡

*Department of Geological Sciences, Queens University, Kingston, ON K7L 3N6, Canada
†Department of Geology, Colorado College, Colorado Springs, CO 80903, USA
‡Department of Earth and Planetary Sciences, MSCO3-2040, 1 University of New Mexico, Albuquerque, New Mexico 87131-0001, USA

(*Received* 31 August 2007; *accepted* 14 January 2008)

Abstract – A newly investigated travertine deposit in southern Tibet provides a window into Holocene hydrological, geomorphic and climatic processes near the boundary of the Tibetan Plateau and High Himalaya. Travertine, deposited as a result of the degassing of CO_2-rich groundwater as it emerges on the Earth's surface, is in many cases formed along the trace of major crustal-scale faults in primarily extensional tectonic regimes. A travertine platform measuring roughly 1 km by 0.5 km exists near the town of Nyalam in southern Tibet along a major Himalayan down-to-the-N normal fault, the South Tibetan Fault System. A wide variety of travertine depositional textures and features are recorded in the platform on a series of terraces. Active travertine deposition was observed from spring mounds and seeps along the base of the platform at the modern river level. Palaeotemperatures of spring water, calculated from $\delta^{18}O$ of the travertine, range from 9 to 25 °C, which closely matches the temperatures recorded from modern springs in the area. A complex geomorphological landscape records interaction between growing alluvial fans, travertine accumulation, and a rapidly down-cutting river with associated fluvial terraces. River incision was contemporaneous with travertine deposition, as indicated by cemented fluvial river gravel layers interbedded with travertine. High $^{87}Sr/^{86}Sr$ ratios in the travertine (mean of 0.7168) indicate subsurface fluid interaction with radiogenic crystalline rocks of the underlying Greater Himalaya. Uranium-series ages of the travertine platform range from 5400 a (± 950 a) to 11 600 a (± 1000 a), and indicate a younging progression from higher terraces near the valley wall to lower terraces at present-day river level. Travertine that overlies a river gravel terrace 18 m above river level formed at 11 600 a. This date yields a local incision rate of 1.6 mm a^{-1}, consistent with estimated fluvial incision rates in the High Himalaya. The range of our U-series ages coincides with an interval of higher precipitation associated with greater intensity of the Indian monsoon, which led to elevated spring discharge and carbonate precipitation in this part of the High Himalayas.

Keywords: travertine, Tibet, Sr-87/Sr-86, geochronology, Himalayas.

1. Introduction

Travertine deposits provide unique records of hydrological systems. Although travertine is common worldwide in a variety of hydrological settings, of particular interest are those occurrences linked to tectonic activity and extensional fault systems (Barnes, Irwin & White, 1978; Hancock *et al.* 1999), such as many deposits in the western USA (Chafetz & Folk, 1984; Newell *et al.* 2005; Crossey *et al.* 2006). The geochemistry of travertine-depositing mineral springs along major structural features suggests that deeply sourced, or endogenic, CO_2-rich water exploits faults and fractures and later travels to the surface (e.g. Yoshimura *et al.* 2004). This acidic water dissolves surrounding carbonate rock so that, upon reaching the surface, it degasses and leads to precipitation of carbonate in the form of travertine. Present models of hydrological systems that source travertine springs include mixing of varying proportions of shallowly circulated meteoric (epigenic) water with deeply sourced and circulated endogenic water (Crossey *et al.* 2006). In these models, small contributions (a few per cent) of deeply sourced water can significantly influence the geochemistry of a groundwater body (Newell *et al.* 2005; Crossey *et al.* 2006).

In addition to being a regional indicator for tectonic activity and hydrological variation, travertine deposits considerably impact the local geomorphology in the landscapes where they occur. They can locally reduce the sediment budget of fluvial systems by mantling relict fluvial deposits and entombing sediment so that it cannot be eroded. Travertine deposits have the potential to alter the course of a river by prograding across a river floodplain, thereby restricting the flow path of the river. Some travertine deposits partially or fully dam rivers, such as Soda Dam in New Mexico (Goff, 1987). This damming can cause lakes to form upriver of the travertine, or can cause avulsion of the riverbed (Pentecost, 1993; Ford & Pedley, 1996). Also, since travertine can be dated using U-series

†Author for correspondence: pmyrow@coloradocollege.edu
‡Current affiliation: Hydrogeology, Geochemistry and Geology Group, Los Alamos National Laboratory, Los Alamos, NM 87545, USA

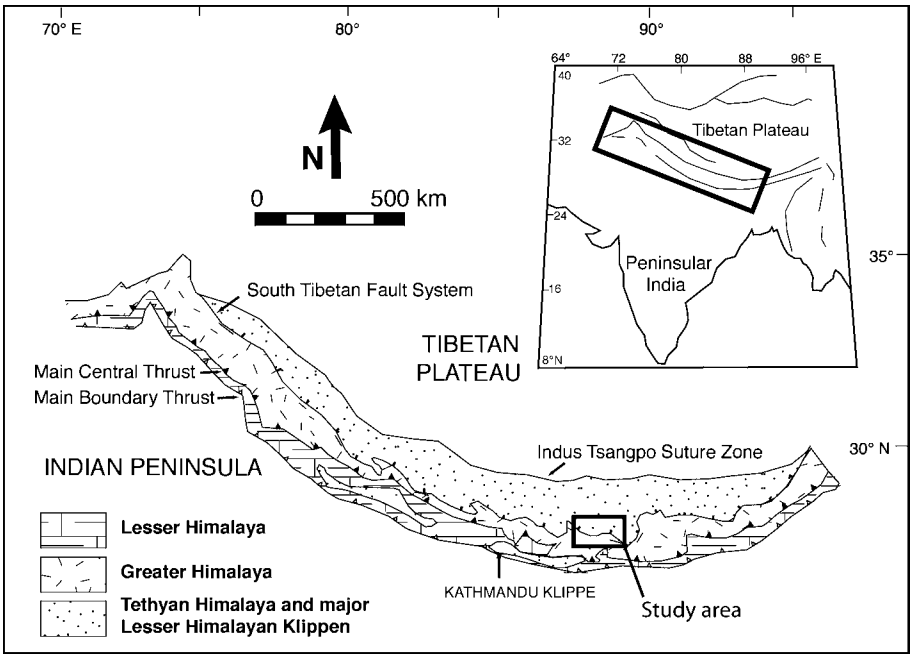

Figure 1. Regional lithotectonic map of the Himalaya with study area located approximately 30 km north of Nyalam, Tibet indicated in black box (after Myrow *et al.* 2003).

geochronology, these deposits can be used as a chronological constraint on geomorphic features, such as river terraces (Pederson *et al.* 2002).

Herein we present data on a newly discovered travertine deposit that is located within the Tethyan Himalayan lithotectonic zone (Fig. 1), near the contact between the Tethyan and the high-grade crystalline rocks of the Greater Himalaya (Fig. 2). The travertine occurs along the trace of the upper strand of the South Tibetan Fault System, which is a major normal fault system that marks the southern boundary between the Tethyan and Greater Himalaya. We herein describe the characteristics of this travertine deposit, outline the geomorphological effects of travertine deposition, provide Sr isotope data of the travertine and the implications for fluid flow, and finally, provide uranium-series ages for the deposit that illustrate the manner in which it developed, and that potentially link travertine deposition to Holocene climate variability. This is the first known study for this region of the Tibetan Plateau. Previous work on travertine systems in Tibet include geochemical studies on active springs on the Tibetan Plateau further to the NE (Hoke *et al.* 2000; Yokoyama, Nakai & Wakita, 1999), and one study dating travertine from Tingri, about 120 km northeast of Nyalam, that yielded an age of 100 ka (Sweeting, Bao & Zhang, 1991).

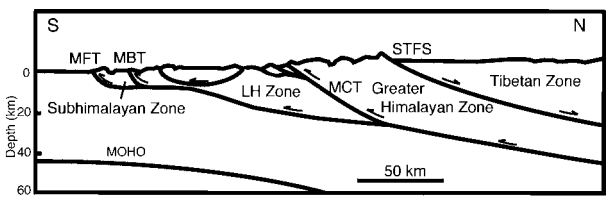

Figure 2. Simplified structural cross-section of the Himalaya. STFS – South Tibetan Fault System, MCT – Main Central Thrust, MBT – Main Boundary Fault, MFT – Main Frontal Thrust.

2. Geological history

In southern Tibet, along the northern flank of the Himalaya, Neoproterozoic to Eocene marine deposits of the Tethyan Himalaya lie in contact with the crystalline rocks of the Greater Himalaya (Fig. 2) across the South Tibetan Fault System. Tectonic fabrics and structures in the rocks of the Greater Himalaya, and E–W-trending, S-vergent folds in the Tethyan strata, indicate an initial phase of southward transport along the South Tibetan Fault System consistent with crustal shortening (Burchfiel *et al.* 1992). Subsequent extension occurred through low-angle, N-dipping normal faults (Hodges, 2000) and, potentially, through channellized flow of partially molten lower Tibetan crust (Bird, 1991; Royden, 1997; Nelson, 1996; Searle, Law & Jessup, 2006). Movement along the South Tibetan Fault System normal faults is predominantly down-dip to the north, although many locations also show oblique displacement (Pecher, 1991; Coleman, 1996).

The South Tibetan Fault System is well exposed at the study area north of Nyalam, Tibet. Here, the fault strikes NE and dips NW 20 to 30°, and cuts hanging-wall bedding at low angles (Burchfiel *et al.* 1992). This fault rests in the same structural and stratigraphic position as the Qomolangma Detachment, the upper of two strands of the South Tibetan Fault System in the Everest region (Searle, 1999; Searle *et al.* 2003). The footwall is made up of an injection complex of Cambrian quartzite and psammitic schist of the

Rouquiecun Group (Burchfiel *et al.* 1992). High-grade metamorphic rocks of the Rongbuk Formation underlie these strata across the lower strand of the South Tibetan Fault System, the Lhotse detachment (Searle, 1999; Searle *et al.* 2003). All of these units are well exposed in the area and they have no travertine associated with them. Above the Rouquiecun strata, and just below the Qomolangma Detachment, is a 109 m thick foliated yellow- to orange-weathering, highly sheared limestone, which in the Everest region is commonly referred to as the 'Yellow Band' (Jessup *et al.* 2006). Above the fault contact on the hanging-wall is a thick succession of Ordovician limestone of the lower Chiatsun Group. The lower 105 m consists of intensely fractured blue-weathering limestone, and this is followed by 65 m of pink- to white-weathering deposits of a thrombolite reef complex.

3. Location

The travertine deposit described in this study is located on the NE side of a steeply incised river valley approximately 30 km north of Nyalam in southern Tibet. The valley is accessible by a dirt road that branches off the Friendship Highway to the west (Fig. 1), and the road crosses the travertine platform approximately 5 km west of the mouth of the valley (Fig. 3).

The valley contains a high-energy braided stream that has cut down through bedrock and alluvial fan deposits. The fluvial deposits consist of winnowed gravel and cobble terraces. On the NE side of the river, river terraces are partially covered by alluvial fans that emanate from the steep valley wall. On the SW side of the river, river terraces are not extensive and in several places the river is in contact with vertically incised bedrock. Less than a kilometre upriver from the study area the valley widens considerably and the stream gradient lessens, so the study area represents a knickpoint in this fluvial system. This knickpoint also corresponds to where the upper strand of the STFS crosses the valley, juxtaposing the brittlely deformed Ordovician strata against ductilely deformed Cambrian sedimentary rocks. At this transition, there is a cliff about 100 m high where an alluvial fan on the southwest side of the valley is cut by the river. The surface of that fan projects to a similarly oriented surface across the valley to the northeast (Fig. 3).

The travertine platform is situated along the northeastern valley wall beneath outcrops of Ordovician carbonate. Only minor travertine deposits exist near the present river level on the southwest side of the river. Spring discharge was observed as seeps below the travertine platform on the northeast side of the river and from spring mounds on the southwest side of the river, and these springs were associated with recent travertine accumulations. Similar travertine deposits and active springs were observed, but not described by this study, along the Friendship Highway north of the study area and south of the ascent onto the Tibetan Plateau (N28°22.957, E086°6.507, 4376 m).

4. Methods

Samples were collected from sites across the platform, and from adjacent Ordovician limestone bedrock, for geochemical and petrographic analysis. In order to describe the morphology of the platform, we used a tape, Jacob staff and a level to conduct nine parallel cross-sections between the river and the valley wall (Fig. 4). These cross-sections were linked by a perpendicular transect that stretched the length of the platform. Along each cross-section we made careful descriptions of lithologies and textures. A brief description of the travertine textures of the platform are provided, but a detailed petrographic and petrological analysis is beyond the scope of this paper.

Powdered samples of travertine were analysed for mineralogical composition on a semi-automated X-ray diffractometer at Colorado College, and for carbon and oxygen isotopic analyses on a continuous flow Finnegan Mass Spectrometer at Colorado Plateau Stable Isotope Laboratory at Northern Arizona University. Strontium isotope analysis of ten travertine samples was carried out at the University of Illinois, Champaign–Urbana, using a Nu Plasma multi-collector ICP-MS. Samples representing a broad spatial distribution across the travertine platform and a variety of travertine textures were selected for ^{87}Sr–^{86}Sr analysis. A sample of Ordovician limestone taken in the cliff face above the travertine platform was also analysed. Small pieces of travertine were picked off each sample, powdered and dissolved in acid. The samples were then centrifuged to remove impurities, siliciclastic grains and clay minerals. They were flushed through columns of resin with strong acid to selectively leach strontium. Each sample was diluted and analysed on a plasma mass spectrometer for $^{87}Sr/^{86}Sr$ ratio.

Six samples of travertine were analysed at the University of New Mexico's Radiogenic Isotope Laboratory for U-series ages. For each sample, a small volume of travertine powder was drilled out of the most indurated layer that contained a minimum of siliciclastic material. Powdered travertine was dissolved in HNO_3 and spiked with a mixture of ^{229}Th–^{233}U–^{236}U. Anion exchange columns were used in two runs to separate U and Th after they were co-precipitated with pure $FeOH_3$. Isotopic ratios were determined using a Micromass Sector 54 thermal ionization mass spectrometer (TIMS) with a high-abundance sensitivity filter and an ion-counting Daly multiplier. Age uncertainties in the ratios are 2 sigma of the mean and include those related to initial $^{230}Th/^{232}Th$ correction ($4.4 \times 10^{-6} + 50\,\%$) (Polyak & Asmerom, 2001). Data for the U-series analyses can be obtained from the authors upon request.

5. Mesoscopic features

It is not evident from the field relationships whether the spring water that deposited the travertine platform emanated from one spring source or from several sources. The platform is characterized by a number of extensive

Figure 3. Photomosaic of travertine platform and T1 – Terrace 1, T2 – Terrace 2, AFT – alluvial fan toe.

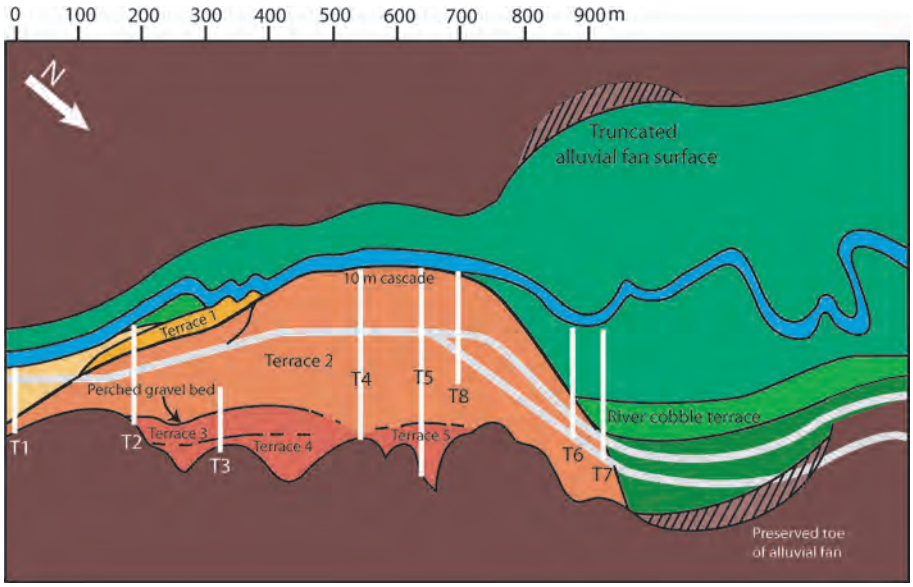

Figure 4. Map view of field area. Travertine platform is shown in orange, yellow and red. T1 through T8 are cross-sections, and grey lines are roads. Scale along top edge is distance in metres.

terraces (cf. Mammoth hot springs: Chafetz & Guidry, 2003), across which variable chemical and physical conditions produced a wide variety of typical small- and large-scale travertine textures. One such texture (Fig. 5b) is defined by a series of 1–1.5 cm thick undulatory layers with granular and bladed calcite crystals that are locally arranged into poorly structured fans. Oncoids or pisoids (Guo & Riding, 1998; Ford, 2003) are also present as nonaligned, concentrically laminated spheres that range from 1 to 15 mm in diameter (Fig. 6a). Foam rock (*sensu* Chafetz & Folk, 1984) is present as networks of holes 2–3 mm in diameter on the upper surface of some travertine layers (Fig. 5d). The majority of carbonate at this site is laminated. Lamination styles include (1) repetitive layers of massive carbonate, (2) heteropachous alternations of light and dark laminae (Fig. 6c), and (3) cyclic repetition of dark laminae, micrite and crystal rays (Fig. 5b) (Pentecost, 2005).

Dams are present at all scales. Microdams coat a variety of surfaces from near-horizontal to near-vertical (Fig. 5a). They are small, often parallel but sometimes anastomosing, stepped-down ridges with undulating crestlines. Each microdam is approximately 5 mm wide and 2 to 3 mm tall. Interdam distance ranges from 3 mm to several metres. Macrodams, also called terraced mounds (Chafetz & Folk, 1984), rimstone pools (Warwick, 1953) and terracettes (Bargar, 1978), are shallow, flat pools between 0.5 and 2 metres wide and 1 to 3 metres long, which step down a few centimetres to adjacent pools (Fig. 7), and are commonly covered in microdams. The pools behind the macrodams in many cases contain eroded and redeposited travertine clasts (Fig. 7b). On the travertine platform along the margin

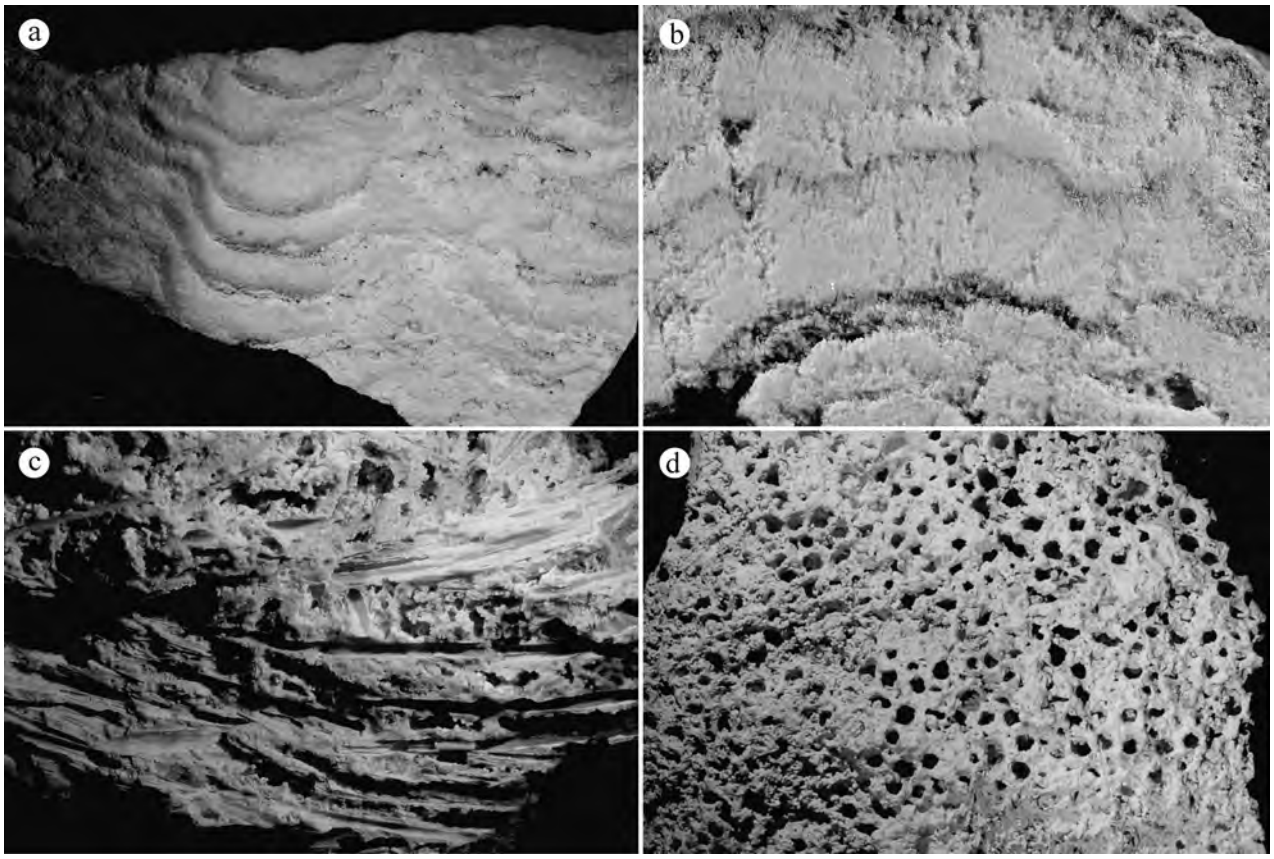

Figure 5. Travertine textures. (a) Microterrace texture (view is 15 cm). (b) Crystalline shrub texture (view is 5 cm). (c) Rhizoliths, specifically, casts of grass blades (view is 5 cm). (d) Sponge-like texture on the upper surface of a layer of travertine (width of field of view is 10 cm).

of the alluvial fans, large blocks of bedrock are found surrounded by travertine (Fig. 8). The blocks range from 0.1 to 0.5 m in diameter. Some blocks are resting on top of the travertine as float (Fig. 8b), some are partially surrounded by travertine (Fig. 8a), and others are completely entombed within the travertine (Fig. 8c). Carbonate overgrowths on grass blades and plant stems (Pedley, 1987; Guo & Riding, 1998; Klappa, 1980) confirm the presence of macrophytes during active deposition. These are observed *in situ* on a cliff face of travertine, 1 m above the present river level (Fig. 9a), and approximately 45 m southeast of the point where Transect 4 meets the river (Fig. 4). The shape and size of these encrustations (Fig. 5c) match those of living plants along the edge of the river.

A 1 m thick fluvial gravel bed exists at the base of Terrace 3, 18 m above the modern river level (Fig. 9c). The bed consists of clast-supported gravel, the basal 30 cm of which contains cobbles and boulders. The upper 70 cm of the bed is made up of poorly sorted sand- to boulder-sized gravel with rounded to subangular clasts. Platy clasts show excellent imbrication, indicating palaeoflow direction predominantly to the southeast, parallel to the modern river flow. Large, locally derived clasts, which contain part of both the top of the gravel bed and some travertine that mantled the gravel, exist on top of Terrace 3. These clasts, up to approximately 1 m long on their intermediate axes, exhibit grass encrustations in a matted texture (Fig. 9b).

At locations where travertine terraces end and abruptly step down to a lower level, layers of laminated travertine drape the sharp change in slope. These cascade or waterfall facies (cf. Guo & Riding, 1998) are preserved in some places on the edge of Terrace 2 (Fig. 10c), and are well exposed at the cliff where Terrace 4 meets the present river gravel bars (Fig. 10a, b). The cascade at Terrace 2 is between 0.5 and 1 m high. The cascade on the Terrace 4 cliff along the river is 10 m high at its highest point and appears to have mantled and prograded outwards from a 10 m tall fluvial gravel terrace that extends out from Terrace 4 to the NNW. The cascade features represent travertine deposition over the pre-existing topography of fluvial terraces. This is evident from the mantling of Terrace 2 over the large gravel terrace that extends NNW along the river.

6. Geomorphology

The travertine platform is located at a narrowing and steepening of the valley that corresponds with a knickpoint formed by the transition from brittlely deformed carbonate strata to ductilely deformed Cambrian rocks, across the upper strand of the South Tibetan Fault System. The growth of the travertine platform radially from a source or sources on the NE

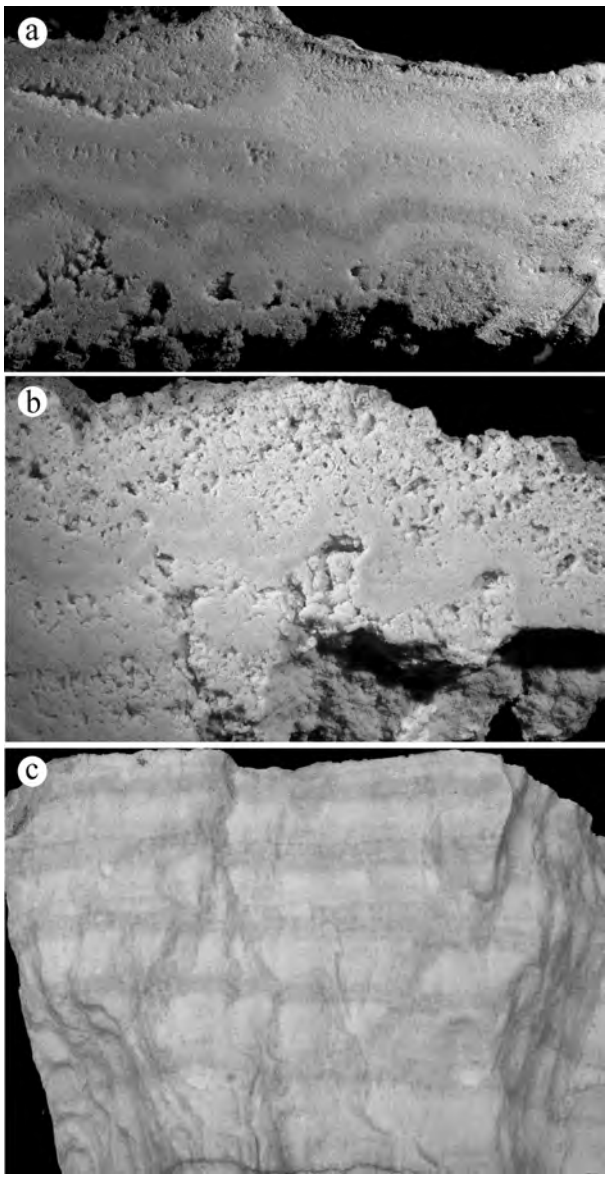

Figure 6. (a) Globular texture at the base of a slab (view is 6 cm). Layers of travertine draped over globules. (b) Porous shrub texture with alternating layers of porous and better-indurated calcite (view is 7 cm). (c) Clean carbonate texture (width of field of view is 10 cm).

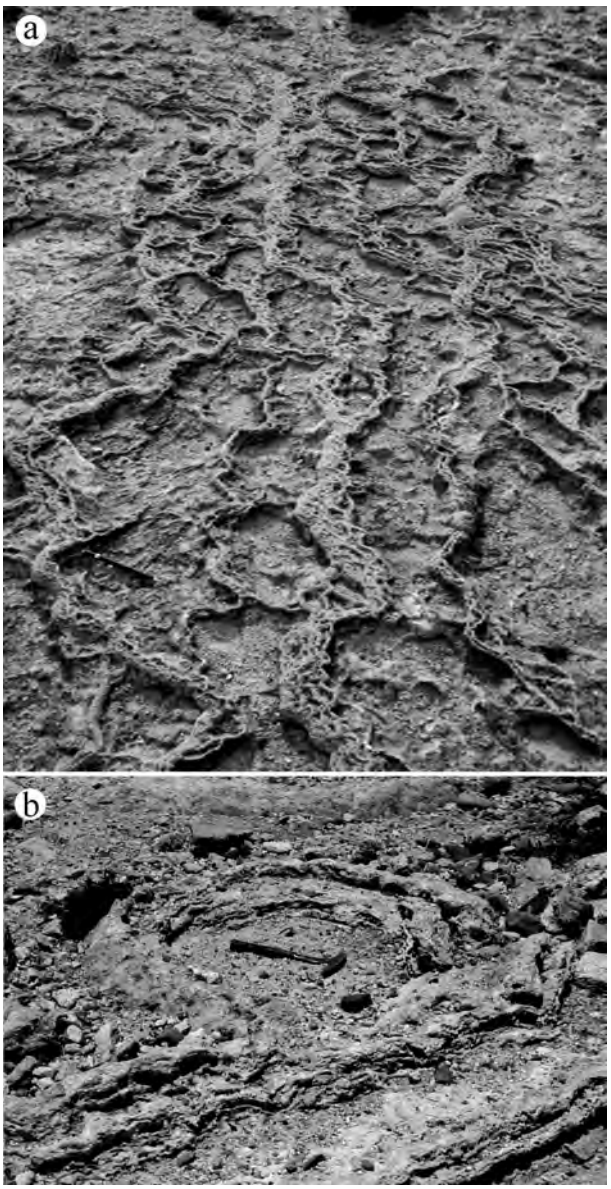

Figure 7. Pools and ridges. (a) Flow direction was right to left and ridges are mantled with microterraces. Pencil is 14 cm long. (b) Large pool with clasts of reworked travertine and adjacent bedrock. Hammer is 37 cm long.

side of the valley has restricted the flow path of the river to a narrow channel pinned along the SW valley wall.

Fluvial and hillslope alluvial processes were incorporated into the travertine platform as active components of the evolving landscape. For instance, the gravel bed at the base of Terrace 3, which is overlain and underlain by travertine, represents a fluvial terrace deposit, based on its clast-supported nature, imbrication, and degree of rounding of the cobbles and boulders. This deposit is similar in character to gravel found along the modern river, and that in a 10 m thick gravel terrace NNW of the travertine platform. The presence of reed and grass encrustations in the large clasts of travertine that also contain river gravel (top of Terrace 3) indicate that the travertine entombed riverbank gravel and macrophytes, a process that is occurring along the banks of the modern river. The perched river gravel at the base of Terrace 3, and these encrustations in the overlying travertine, formed when the ancient channel and riverbank environment was 18–20 m above the current river level. This indicates that there has been at least 18 m of down-cutting during the lifespan of the travertine platform. The subsurface of the travertine platform was not explored in any manner, so it is unclear whether the river cut down through bedrock or previously deposited fluvial deposits, although we presume the latter. Both the perched gravel bed mantled by travertine Terrace 3, and the thick travertine cascade at river level (termination of Terrace 2) that mantles the 10 m thick fluvial gravel terrace deposit, show that travertine deposition and fluvial deposition were contemporaneous and operated over long timescales. In addition, deposition of travertine over these

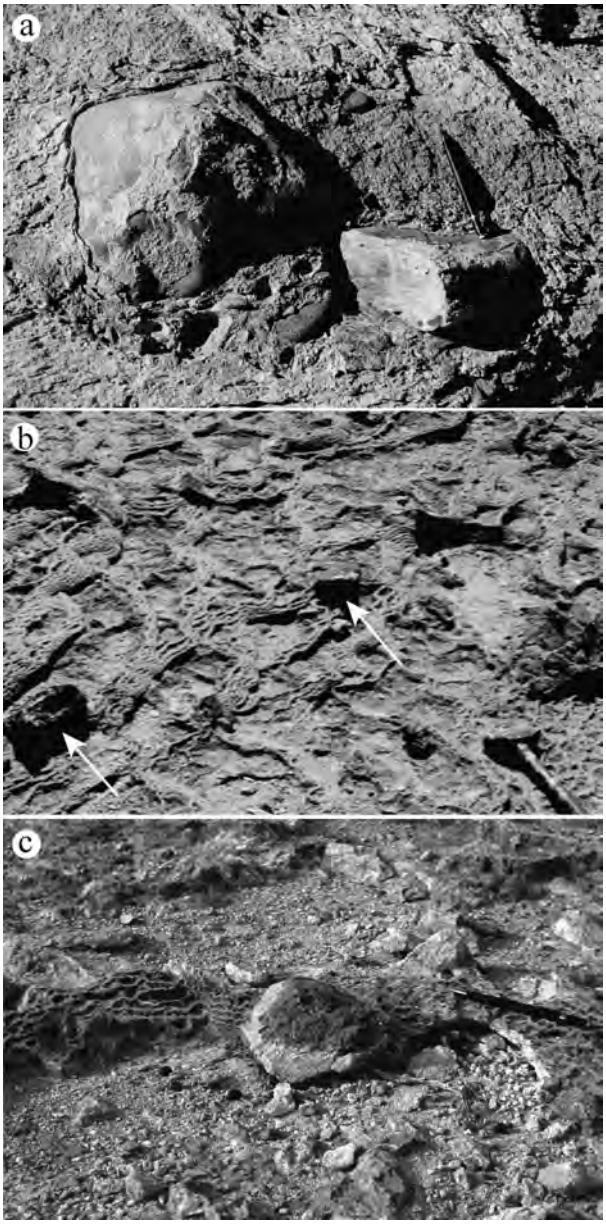

Figure 8. (a) Cobbles encased by travertine. Pencil is 14 cm long. (b) Angular to sub-rounded embedded blocks (arrowed) within pool and ridge textures. These blocks represent rockfall onto an active travertine-depositing flow. Hammer is 35 cm long. (c) Excavated clast with travertine coating (light coloured). Clast removed from hole below pencil.

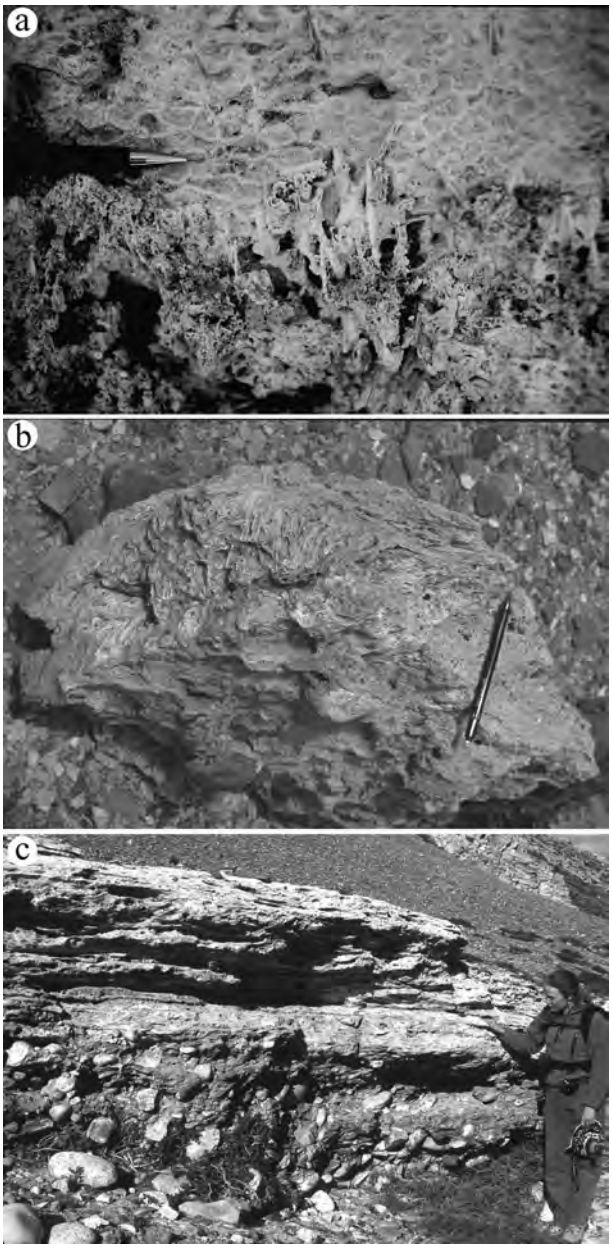

Figure 9. (a) Rhizoliths in travertine beside the river. (b) Clast with rhizoliths and travertine-covered cobbles above Terrace 3 gravel bed. (c) Gravel bed underlain and overlain by travertine. Note rounded clasts and imbrication indicating flow from left to right.

gravel terrace treads entombed them and shielded them from further erosion. This process likely influenced the river's sediment budget during the long-term progradation of the platform. These processes are observed today, where the active spring seeps and mounds at river level are cementing modern river gravels.

Erosion and deposition along the walls of the valley also affected the travertine platform. In addition to the embedded rock falls described above, the toes of alluvial fans on the NE side of the valley locally prograded over the proximal parts of the platform (Figs 3, 4). The toe of a large alluvial fan that prograded from the southwest side of the river, and was later incised by the river, also rests on the platform (Figs 3, 4). Based on the present position of the river, and the fact that the terminus of the terrace is not eroded, as the travertine prograded across the river valley it forced the river to the far side of the valley (Fig. 3, 4). All of the features described above illustrate the potential for a travertine system to drastically influence a host of geomorphological processes.

7. Geochemistry

X-ray analysis indicates that all samples are entirely composed of low-Mg calcite. Complete analytical data for the ^{87}Sr–^{86}Sr and stable isotope analyses are availabale from the authors, and summary data are

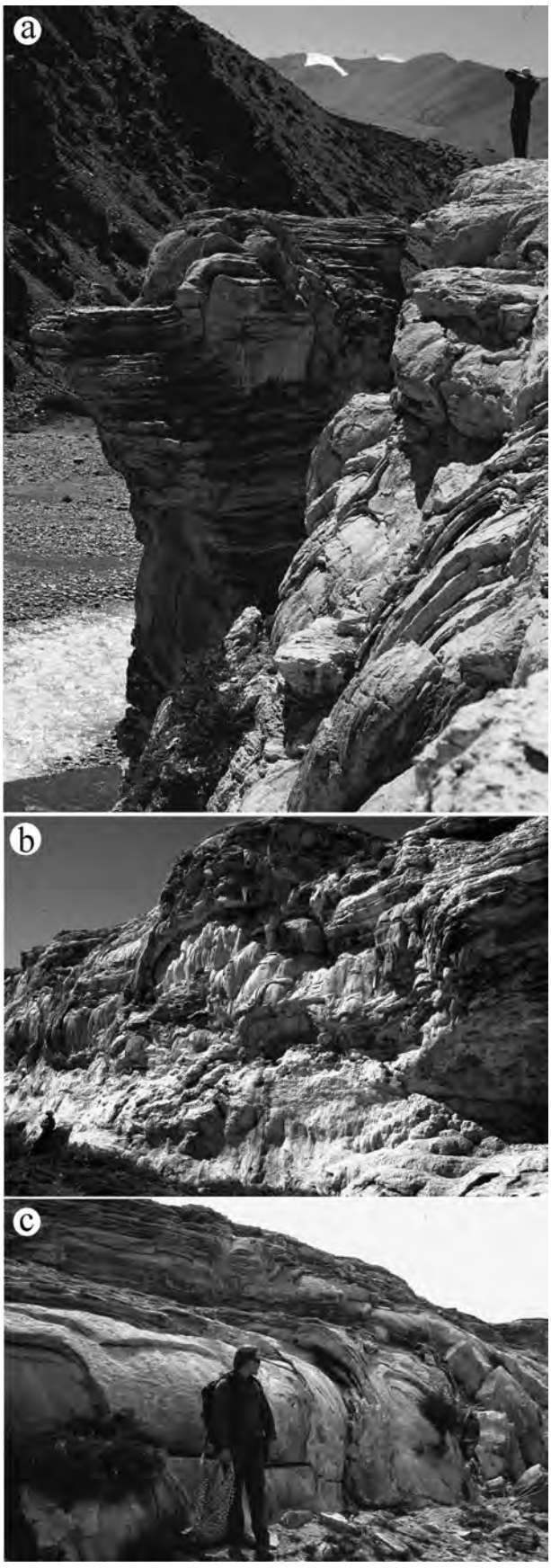

Figure 10. Cascades. (a) 10 m tall cascade cliff at Transect 4 with metre-scale folds. Person for scale in upper right. (b) Face of large cascade cliff shown in (a). Folds with vertical travertine on the left; eroded face of cliff on right. This surface is the terminus of the travertine platform. Person for scale in lower left. (c) Well-developed cascade on Terrace 2.

given in Table 1. δ^{13}C values range from 4.73 to 7.66 ‰(PDB) and δ^{18}O values range from −14.45 to −20.17 ‰(PDB). The relatively high δ^{13}C values rule out alteration by interaction with soil CO_2, as expected given the minimal soil development on the landscape. Fractionation (several per mil) to slightly higher values may have resulted either from evaporation or progressive degassing of CO_2 during surface flow across the platform. The δ^{18}O values for the travertines range from −20.2 to −14.5 ≈ (PDB). Using carbonate-water palaeothermometers (O'Neil, Clayton & Mayeda, 1969; Epstein *et al.* 1953), palaeotemperatures for the springs are estimated to range from ∼ 9 to 25 °C. For the calculation, we assume that meteoric water has not varied significantly over the Holocene and is representative of past spring water. Published δ^{18}O values for High Himalayan rivers at elevations above 3000 m (−16 to −19 ≈ v. SMOW) (Gajurel *et al.* 2006) are used as a proxy for local meteoric water. The calculated temperatures are consistent with active springs at the site (Newell *et al.* unpub. data), suggesting that the oxygen isotopes have not been significantly altered by diagenesis and that the springs responsible for the travertine platform were cool springs.

^{87}Sr/^{86}Sr ratios from the travertine platform range from 0.7169 to 0.7181 (Fig. 11; Table 1), and the Ordovician limestone has an ^{87}Sr/^{86}Sr ratio of 0.7112. The isotopic ratio of ^{87}Sr/^{86}Sr in a travertine reflects the geochemistry of the rocks through which the source fluids passed. In this area, the most likely source of carbonate is the steeply dipping Ordovician limestone in the hanging-wall of the South Tibetan Fault System, which is exposed directly above the platform and which extends deeply into the subsurface. Marine carbonate acquires the ^{87}Sr/^{86}Sr ratio of the seawater in which it forms (Veizer & Compston, 1974). The fluctuation in ^{87}Sr/^{86}Sr ratio in the global oceans through the Phanerozoic has been documented through analysis of marine carbonate, evaporite and phosphorite (Burke *et al.* 1982; Palmer & Elderfield, 1985; Elderfield, 1986; Veizer, 1989). ^{87}Sr/^{86}Sr ratios ranged from 0.7090 in the Early Ordovician to 0.7079 in the Middle to Late Ordovician (Burke *et al.* 1982). Thus, the isotopic value (0.7112) from our Ordovician bedrock sample is

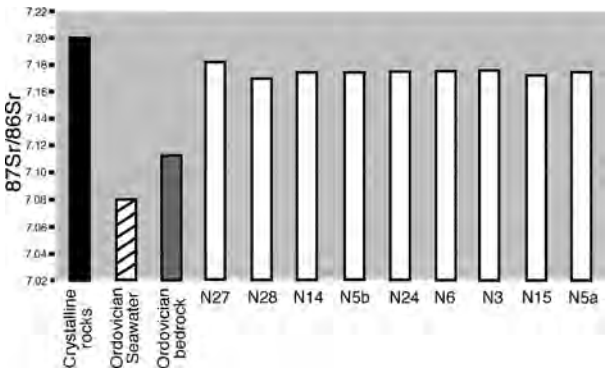

Figure 11. ^{87}Sr/^{86}Sr ratios for sampled travertine, local Ordovician bedrock, average Ordovician seawater, and an estimate for crystalline rocks in the area (from Faure & Powell, 1972).

Table 1. $\delta^{18}O$ and $\delta^{13}C$ isotopic composition, $\delta^{234}U$ isotopic composition, calculated ages in years, and $^{87}Sr/^{86}Sr$ of the travertine

Sample	$\delta^{13}C$ VPDB (‰)	$\delta^{18}O$ VSMOW (‰)	$\delta^{234}U$	Calculated age (years)	$^{87}Sr/^{86}Sr$
N3	5.36	11.26			0.7175161
N5	6.64	12.12			0.7174082
N6	5.18	11.13			0.7174424
N14	4.75	10.12	-34.7 ± 4.7	6816 ± 336	0.7173969
N15	4.85	12.50			0.7171186
N24	7.66	12.27	-35.7 ± 4.3	6507 ± 471	0.7173925
N25			-38.2 ± 3.6	5409 ± 950	
N27	6.85	16.02			0.7181706
N28	4.73	13.12	-46.5 ± 7.1	11401 ± 308	0.7169021
TB-16			-36.3 ± 6.3	8993 ± 420	
TB-17			-57.0 ± 4.9	11654 ± 1017	

anomalously high for marine carbonate, including the average for Ordovician strata. The isotopic values of the travertine (0.7169 to 0.7181) are even higher than those of the Ordovician bedrock. This eliminates the possibility that the spring was fed directly by meteoric waters that only dissolved limestone bedrock. The radiogenic nature of the travertine Sr isotopic ratios indicates that somewhere on the flow-path, spring waters passed through radiogenic bedrock. Siliciclastic and metasedimentary deposits are generally associated with high Sr ratios due to the radioactive decay of ^{87}Rb to ^{87}Sr. Sr ratios range from 0.702 to > 0.780, depending on the age of the rocks and their composition (Faure & Powell, 1972; McNutt, 2000). The rocks of the Greater Himalaya, an injection complex of Neoproterozoic psammitic schist and leucogranite (Rongbuk Formation), as well as the Cambrian quartzite and psammitic schist in the footwall of the South Tibetan Fault System, would contribute a radiogenic signature to fluids passing through them.

In this study we present two possible end-member fluid-flow models (Fig. 12). In the first, meteoric water travelled to depth and was then brought to the surface along a fracture or fault system, possibly related to the South Tibetan Fault System. In the second model, meteoric water percolated down through the highly fractured Ordovician limestone and mixed with rising endogenic fluids from a deeper hydrological system that was in equilibrium with Greater Himalayan crystalline bedrock. Endogenic fluids can arise from deep sources, including geothermal systems related to magmatism, mantle devolatilization and crustal metamorphism, and mixing of even small amounts can significantly alter the geochemistry of travertine-depositing mineral springs (Liu *et al.* 2003; Crossey *et al.* 2006). Both hydrogen and oxygen isotopic analyses of present-day spring water at the study site indicate that it is mostly meteoric (Newell, unpub. data), so that endogenic input is in fact volumetrically minor. The disproportionately large effect of small volumes of endogenic fluid has been shown to be important for travertine developed along prominent fault zones in the southwest USA (Newell *et al.* 2005; Crossey *et al.* 2006). Both models imply that all or a portion of the fluid would have

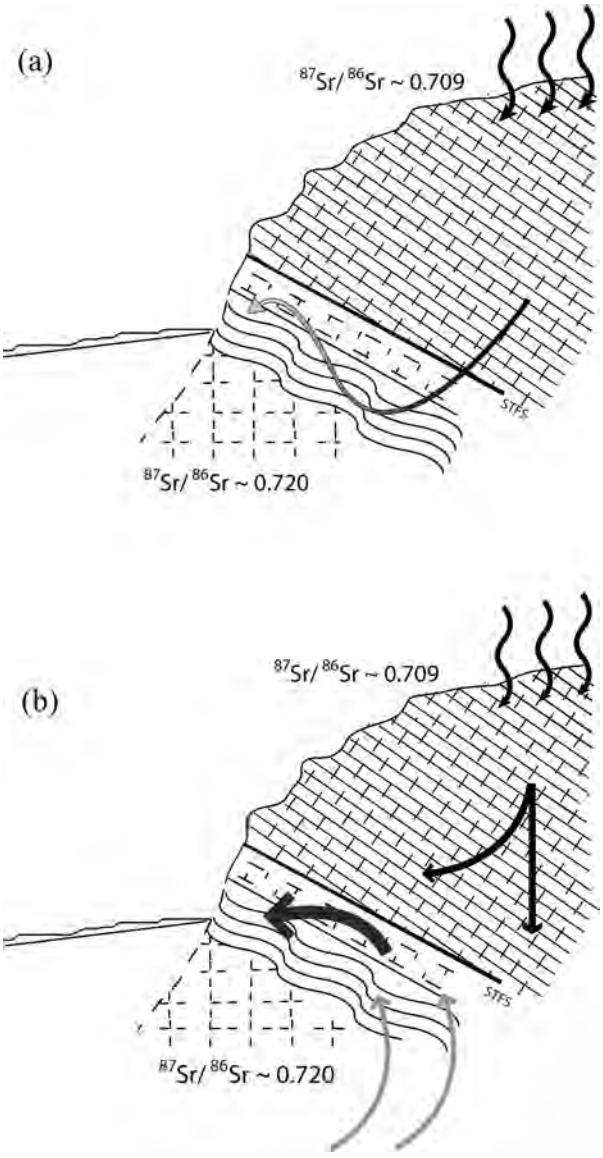

Figure 12. End-member models for the hydrological system that fed the travertine depositing spring. (a) Surface water reached shallow depths, and acquired a radiogenic isotopic signature from interaction with Greater Himalayan rocks. STFS – South Tibetan Fault System. (b) Small volume of endogenic water rising along the South Tibetan Fault System from great depth passed through the Greater Himalayas and mixed with meteoric waters to produce elevated $^{87}Sr/^{86}Sr$ ratios.

interacted with the Greater Himalayan crystalline rocks that lie below the Tethyan Himalayan sedimentary sequence in the footwall of the South Tibetan Fault System.

Intermediate values for the Ordovician limestone suggest that it has been diagenetically altered. The limestone is highly fractured to allow for fluid flow. Therefore, it is likely that fluid carrying a radiogenic signature due to interaction with the Greater Himalayan rocks may have permeated the limestone along fractures and faults, and elevated its $^{87}Sr/^{86}Sr$ ratios.

The thick accumulation of travertine implies movement of CO_2-charged waters, and their degassing at the surface (Zhang, Zhang & Zhu, 2001; Chen *et al.* 2004). One possible source of the CO_2 is biological degradation of organic matter in soils. However, the relatively dry climate and very poor soil development in this region, in combination with the high $\delta^{13}C$ values for the travertine, rule out this possibility. Candidate processes posed for other mineral springs, including those in the Tibetan Plateau, include metamorphic decarbonation of carbonate rocks, magmatism, or mantle devolatilization (e.g. Hoke *et al.* 2000; Yoshimura *et al.* 2004; Newell *et al.* 2005). The lack of present-day magmatism and the extremely thick crust in the region argues against the presence of significant mantle fluids. High carbon isotope values support our interpretation for the input of the CO_2 from crustal metamorphic decarbonation reactions.

Basement-penetrating normal faults are often associated with travertine deposits (Barnes, Irwin & White, 1978; Hancock *et al.* 1999). In our study area, a travertine platform accumulated along the strike of the Qomolangma Detachment, the upper strand of the South Tibetan Fault System, where it crosses a river valley, precisely where Ordovician carbonate rocks of the Tethyan Himalaya crop out in the hanging-wall. CO_2-charged fluids utilized the South Tibetan Fault System as a fluid pathway, dissolving carbonate rocks along the fault zone and redepositing them as travertine at the surface. Deep penetration of the South Tibetan Fault System into high-grade rock of the Greater Himalaya may have allowed for mixing of high-volume meteoric recharge with more deeply sourced CO_2-charged endogenic water, similar to what has been documented in the southwestern USA (Newell *et al.* 2005). Circulation of surface water to relatively shallow depths in the footwall of the South Tibetan Fault System could also have elevated the isotopic ratios, but this is unlikely because it does not explain the high levels of deeply sourced CO_2 needed in the spring water to produce the travertine.

8. U-series dating

The travertine samples range in age from 5400 a (± 950 a) to 11 600 a (± 1000 a) (Fig. 13). The oldest travertine sample, N28, was taken relatively proximal to the likely source spring(s), from a high elevation on the platform (6 m below the highest recorded travertine). It was collected from the top of Terrace 3, southeast of Transect 3, and records a U-series age of

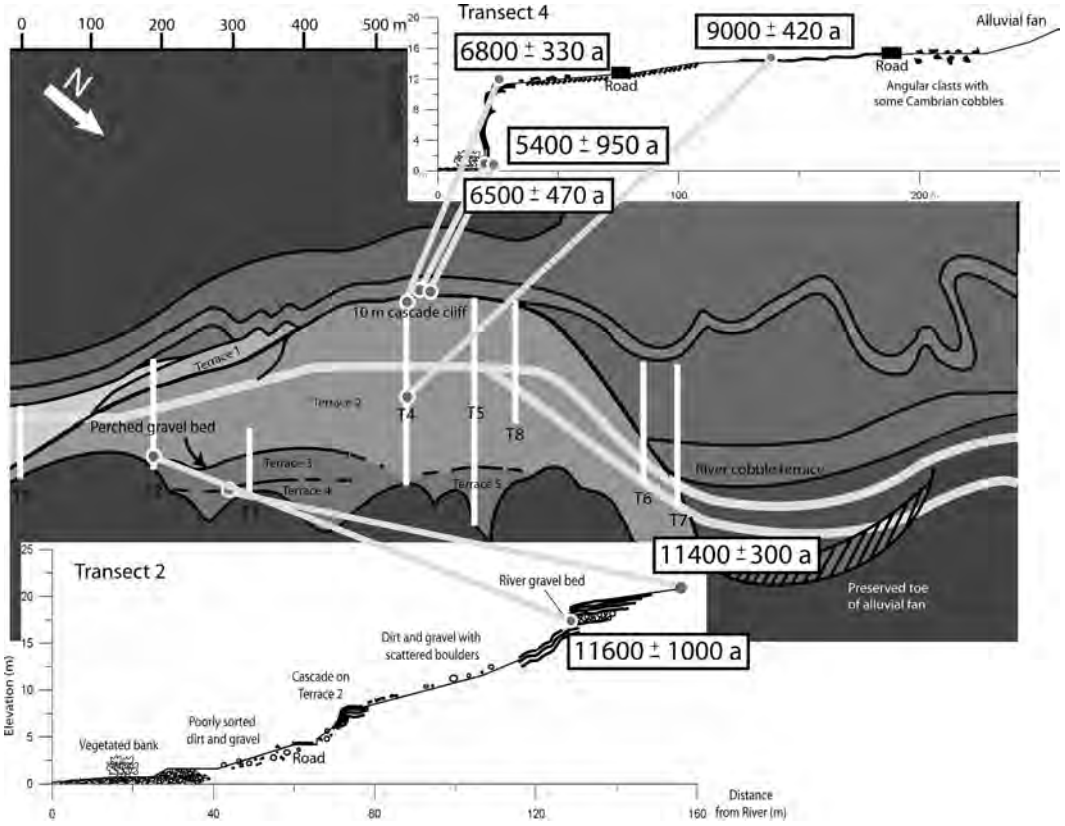

Figure 13. Map of sampling locations with associated U-series dates. Scale along top edge is distance in metres.

11 400 a (± 300 a) (Fig. 13). Sample TB17 was taken from the top of the perched gravel bed along Transect 3, approximately 1 m stratigraphically below N28, and its calculated age is 11 600 a (± 1000 a). Sample TB16, collected from the top of Terrace 2, yielded an age of 9000 a (± 420 a). Sample N14 was collected at the top of the 10 m tall cascade on Transect 4 and records an age of 6800 a (± 330 a). Two samples, N24 and N25, were taken from the most distal part on the platform (closest to present-day river position), at base of this cascade, and these yielded ages of 6500 a (± 470 a) and 5400 a (± 950 a), respectively. In summary, the data show sequentially younger ages moving across the travertine platform from the highest terrace against the valley wall toward the present river level.

8.a. Interpretation

The pattern of ages provides insight into the timing and development of the travertine platform. The highest travertine terrace (Terrace 4) on the platform, developed along the valley wall, yielded the oldest U-series ages. Terraces successively lower in elevation and closer to the modern river record progressively younger travertine ages. This pattern suggests that the travertine likely accumulated at the level of the local alluvial water table, initially at higher elevations along the edge of the alluvial fan, and that the spring source migrated as the river incised and local water table dropped. If the spring were fixed at one location, then the platform surface would have been mantled with young travertine and there would be no age progression in surface samples across the platform. Also, present-day spring activity and travertine precipitation is occurring at the stream level. Assuming that the deposition of river gravels and travertine cementation was relatively contemporaneous, the age of the travertine that directly overlies the river gravel of Terrace 3 indicates that the river channel and adjacent ecosystem of reed flora was about 18 m above the present river level at 11 600 a. Although it is not possible to determine if incision since this time was solely within bedrock, these data would suggest a local incision rate of 1.6 mm a^{-1}. Such a rate is reasonable given that fluvial incision rates in the High Himalaya are generally 4–8 mm a^{-1} (Lavé & Avouac, 2001).

The range of uranium-series ages for this travertine platform suggest that the majority of platform growth occurred between 5400 a and 11 600 a. In an arid climate where precipitation rates are low and overland flow is seasonal, it is likely that the bulk of travertine deposition occurred during wet climatic intervals when there was enough water available to allow for relatively high volume flow from the source spring(s). The period between 5400 a and 11 600 a corresponds to a time of higher intensity in the Indian Ocean monsoon (Sirocko, 1993), which could have elevated spring flow in this region of Tibet, and thus increased the volume and/or rate of travertine precipitation. Studies of ocean sediment cores from the Arabian Sea, lake-sediment cores, pollen assemblages, and landslide recurrence intervals in northwestern India, all record elevated precipitation levels during this time interval (Sirocko, 1993; Enzel *et al.* 1999; Singh *et al.* 1974; Bookhagen, Thiede & Strecker, 2005).

9. Conclusions

This study describes a previously undocumented travertine platform north of the town of Nyalam in southern Tibet at the transition from the Tibetan Plateau to the High Himalaya. A broad range of travertine textures (metre- to millimetre-scale) present correlate with those of modern, active travertine springs worldwide (Fouke *et al.* 2000; Pentecost, 2005). Over time, contemporaneous travertine precipitation and fluvial deposition resulted in the cementation and capping of fluvial terrace gravels by travertine, which reduced the river's local sediment budget.

$^{87}Sr/^{86}Sr$ ratios in the travertine require subsurface water–rock interaction with the radiogenic, crystalline rocks, such as those of the Greater Himalaya. We favour a model whereby large-volume meteoric recharge mixed at depth with relatively low-volume CO_2-charged, radiogenic fluids (endogenic fluids), and the mixed fluid utilized the South Tibetan Fault System as a conduit from the crust to the surface. Based on carbon isotopes from the travertine, and given the local crustal thickness, the most likely explanation for the CO_2 source is crustal metamorphic decarbonation reactions.

Uranium-series analysis of travertine from a variety of locations on the platform yielded ages from 5400 a (± 950 a) to 11 600 a (± 1000 a). The ages decrease with decreasing elevation away from the valley wall, towards the modern river, where travertine precipitation was observed. This suggests that travertine deposition may have followed the water table as it was lowered during river incision. A calculated rate of incision of 1.6 mm a^{-1} is close to those calculated for other areas in the High Himalaya. The time interval during which deposition of the main platform occurred corresponds with a period of increased intensity of the Indian Ocean Monsoon, which suggests that deposition may have been related to increased precipitation and an elevated groundwater table. Thus, the travertine in this valley could serve as a record of past climatic changes.

Our work highlights the potential of integrating tectonic, geomorphological, geochemical and palaeoclimatic data for an active tectonic region. The association of travertine with a major tectonic boundary within the Himalayas is striking and warrants further exploration of additional travertine deposits in this relatively unstudied region.

Acknowledgements. This work was supported by the following grants to Paul Myrow: NSF EAR-9980376 and EAR-0543340. We thank Shanchi Peng, Nigel Hughes, S. K. Parcha and Bryan Sell for field and logistical assistance.

References

BARGAR, K. E. 1978. *Geology and thermal history of Mammoth Hot Springs, Yellowstone National Park, Wyoming*. U.S. Geological Survey Bulletin, no. 1444, 1–33.

BARNES, I., IRWIN, W. P. & WHITE, D. E. 1978. *Global distribution of carbon dioxide discharges, and major zones of seismicity*. U.S. Geological Survey: Water Resources Investigations 78–39.

BIRD, P. 1991. Lateral extrusion of lower crust from under high topography, in the isostatic limit. *Journal of Geophysical Research, B, Solid Earth and Planets* **96**, 10275–86.

BOOKHAGEN, B., THIEDE, R. C. & STRECKER, M. R. 2005. Late Quaternary intensified monsoon phases control landscape evolution in the northwest Himalaya. *Geology* **33**, 149–52.

BURCHFIEL, B. C., ZHILIANG, C., HODGES, K., YUPING, L., ROYDEN, L. H., CHANGRONG, D. & JIENE, X. 1992. The South Tibetan detachment system, Himalayan Orogen: extension contemporaneous with and parallel to shortening in a collisional mountain belt. *Special Paper, Geological Society of America* **269**, 4–15.

BURKE, W. H., DENISON, R. E., HETHERINGTON, E. A., KOEPNICK, R. B., NELSON, H. F. & OTTO, J. B. 1982. Variation of seawater $^{87}Sr/^{86}Sr$ throughout Phanerozoic time. *Geology* **10**, 516–19.

CHAFETZ, H. S. & FOLK, R. L. 1984. Travertines: depositional morphology and the bacterially constructed constituents. *Journal of Sedimentary Petrology* **54**, 289–316.

CHAFETZ, H. S. & GUIDRY, S. A. 2003, Deposition and diagenesis of Mammoth Hot Springs travertine, Yellowstone National Park, Wyoming, U.S.A. *Canadian Journal of Earth Science* **40**, 1515–29.

CHEN, J., ZHANG, D. D., WANG, S., TANGFU, X. & RONGGUI, H. 2004. Factors controlling tufa deposition in natural waters at waterfall sites. *Sedimentary Geology* **166**, 353–66.

COLEMAN, M. E. 1996. Orogen-parallel and orogen-perpendicular extension in the central Nepalese Himalayas. *Geological Society of America Bulletin* **108**, 1594–1607.

CROSSEY, L. J., FISCHER, T. P., PATCHETT, P. J., KARLSTROM, K. E., HILTON, D. R., NEWELL, D. L., HUNTOON, P., REYNOLDS, A. C. & DE LEEUW, G. A. M. 2006. Dissected hydrologic system at the Grand Canyon; interaction between deeply derived fluids and plateau aquifer waters in modern springs and travertine. *Geology* **34**, 25–8.

ELDERFIELD, H. 1986. Strontium isotope stratigraphy. *Paleogeography, Paleoclimatology, Paleoecology* **57**, 71–90.

ENZEL, Y., ELY, L. L., MISHRA, S., RAMESH, R., AMIT, R., LAZAR, B., RAJAGURU, S. N., BAKER, V. R. & SANDLER, A. 1999. High-Resolution Holocene Environmental Changes in the Thar Desert, Northwestern India. *Science* **284**, 125–8.

EPSTEIN, S., BUCHSBAUM, R., LOWENSTAM, H. A. & UREY, H. C. 1953. Revised carbonate-water isotopic temperature scale. *Geological Society of America Bulletin* **64**, 1315–26.

FAURE, G. & POWELL, J. L. 1972. *Strontium Isotope Geology*. Berlin–Heidelberg: Springer-Verlag, 188 pp.

FORD, D. 2003. Speleothems. *Encyclopedia of sediments and sedimentary rocks* (ed. G. V. Middleton), pp. 678–81. Kluwer Academic Publishers.

FORD, T. D. & PEDLEY, H. M. 1996. A review of tufa and travertine deposits of the world. *Earth Science Reviews* **41**, 117–75.

FOUKE, B. W., FARMER, J. D., DES MARAIS, D. J., PRATT, L., STURCHIO, N. C., BURNS, P. C. & DISCIPULO, M. K. 2000. Depositional facies and aqueous-solid geochemistry of travertine-depositing hot springs (Angel Terrace, Mammoth Hot Springs Yellowstone National Park, U.S.A.). *Journal of Sedimentary Research* **70**, 565–85.

GAJUREL, A. P., FRANCE-LANORD, C., HUYGHE, P., GUILMETTE, C. & GURUNG, D. 2006. C and O isotope compositions of modern fresh-water mollusk shells and river waters from the Himalaya and Ganga plain. *Chemical Geology* **233**, 156–83.

GOFF, F. 1987. Travertine deposits of Soda Dam, New Mexico, and their implications for the age and evolution of the Valles caldera hydrothermal system. *Geological Society of America Bulletin* **99**, 292–302.

GUO, L. & RIDING, R. 1998. Hot-spring travertine facies and sequences, Late Pleistocene, Rapolano Terme, Italy. *Sedimentology* **45**, 163–80.

HANCOCK, P. L., CHALMERS, R. M. L., ALTUNEL, E. & CAKIR, Z. 1999. Travitonics: using travertine in active fault studies. *Journal of Structural Geology* **21**, 903–16.

HODGES, K. V. 2000. Tectonics of the Himalaya and southern Tibet from two perspectives. *Geological Society of America Bulletin* **112**, 324–50.

HOKE, L., LAMB, S., HILTON, D. R. & POREDA, R. J. 2000. Southern limit of mantle-derived geothermal helium emissions in Tibet: implications for lithospheric structure. *Earth and Planetary Science Letters* **180**, 297–308.

JESSUP, M. J., LAW, R. D., SEARLE, M. P. & HUBBARD, M. S. 2006. Structural evolution and vorticity of flow during extrusion and exhusmation of the Greater Himalayan Slab, Mount Everest Massif, Tibet/Nepal: implications for orogen-scale flow partitioning. In *Channel Flow, Ductile Extrusion and Exhumation in Continental Collision Zones* (eds R. D. Law, M. P. Searle & L. Godin), pp. 379–413. Geological Society of London, Special Publication no. 268.

KLAPPA, C. F. 1980. Rhizoliths in terrestrial carbonates: Classification, recognition, genesis and significance. *Sedimentology* **27**, 613–29.

LAVÉ, J. & AVOUAC, J. P. 2001. Fluvial incision and tectonic uplift across the Himalayas of central Nepal. *Journal of Geophysical Research* **106**, 26561–92.

LIU, Z., ZHANG, M., LI, Q. & YOU, S. 2003. Hydrochemical and isotope characteristics of spring water and travertine in the Baishuitai area (SW China) and their meaning for paleoenvironmental reconstruction. *Environmental Geology* **44**, 698–704.

MCNUTT, R. H. 2000. Strontium Isotopes. In *Environmental Tracers in Subsurface Hydrology* (eds P. G. Cook & A. L. Herczeg), pp. 1–529. Boston/Dordrecht/London: Kluwer Academic Publishers.

MYROW, P. M., HUGHES, N. C., PAULSEN, T., WILLIAMS, I., PARCHA, S. K., THOMPSON, K. R., BOWRING, S. A., PENG, S.-C. & AHLUWALIA, A. D. 2003. Integrated tectonostratigraphic analysis of the Himalaya and implications for its tectonic reconstruction. *Earth and Planetary Science Letters* **212**, 433–41.

NELSON, K. D. 1996. Partially molten middle crust beneath southern Tibet; synthesis of Project INDEPTH results. *Science* **274**, 1684–8.

NEWELL, D. L., CROSSEY, L. J., KARLSTROM, K. E., FISCHER, T. P. & HILTON, D. R. 2005. Continental-scale links

between the mantle and groundwater systems of the Western United States; evidence from travertine springs and regional He isotope data. *GSA Today* **15**, 4–10.

O'NEIL, J. R., CLAYTON, R. N. & MAYEDA, T. K. 1969. Oxygen isotope fractionation in divalent metal carbonates. *Journal of Chemical Physics* **51**, 5547–58.

PALMER, M. R. & ELDERFIELD, H. 1985. Sr isotope composition of sea water over the last 75 Myr. *Nature* **314**, 526–8.

PECHER, A. 1991. The contact between the higher Himalaya crystallines and the Tibetan sedimentary series: Miocene large-scale dextral shearing. *Tectonics* **10**, 587–98.

PEDERSON, J., KARLSTROM, K., SHARP, W. & MCINTOSH, W. 2002. Differential incision of the Grand Canyon related to Quaternary faulting – Constraints from U-series and Ar/Ar dating. *Geology* **30**, 739–42.

PEDLEY, H. M. 1987. The Flandrian (Quaternary) Caerwys Tufa, North Wales; an ancient barrage tufa deposit. *Proceedings of the Yorkshire Geological Society* **46**, 141–52.

PENTECOST, A. 1993. British travertines: a review. *Proceedings of the Geologists Association* **104**, 23–39.

PENTECOST, A. 2005. *Travertine*. Berlin, Heidelberg: Springer-Verlag, 446 pp.

POLYAK, V. J. & ASMEROM, Y. 2001. Late Holocene climate and cultural changes in the southwestern United States. *Science* **294**, 148–51.

ROYDEN, L. H. 1997. Surface deformation and lower crustal flow in eastern Tibet. *Science* **276**, 788–90.

SEARLE, M. P. 1999. Extensional and compressional faults in the Everest-Lohtse massif, Khumbu Himalaya, Nepal. *Journal of Geological Society, London* **156**, 227–40.

SEARLE, M. P., LAW, R. D. & JESSUP, M. J. 2006. Crustal structure, restoration and evolution of the Greater Himalaya in Nepal–South Tibet: implications for channel flow and ductile extrusion of the middle crust. In *Channel Flow, Ductile Extrusion, and Exhumation in Continental Collision Zones* (eds R. D. Law, M. P. Searle & I. Godin), pp. 355–78. Geological Society of London, Special Publication no. 268.

SEARLE, M. P., SIMPSON, R. L., LAW, R. D., PARRISH, R. R. & WATERS, D. J. 2003. The structural geometry, metamorphic and magmatic evolution of the Everest massif, High Himalaya of Nepal – South Tibet. *Journal of the Geological Society, London* **160**, 345–66.

SINGH, G., JOSHI, R. D., CHOPRA, S. K. & SINGH, A. B. 1974. Late Quaternary history of vegetation and climate of the Rajasthan Desert, India. *Philosophical Transactions of the Royal Society of London* **267**, 467–501.

SIROCKO, F. 1993. Century-scale events in monsoonal climate over the past 24,000 years. *Nature* **364**, 322–4.

SWEETING, M. M., BAO, F. S. & ZHANG, D. 1991. The problem of paleokarst in Tibet. *Geographical Journal* **157**, 316–25.

VEIZER, J. 1989. Strontium isotopes in seawater through time. *Annual Review of Earth and Planetary Sciences* **17**, 141–67.

VEIZER, J. & COMPSTON, W. 1974. $^{87}Sr/^{86}Sr$ composition of seawater during the Phanerozoic. *Geochimica et Cosmochimica Acta* **38**, 1461–84.

WARWICK, G. T. 1953. Cave formations and deposits. In *British Caving* (ed. C. H. D. Cullingford), pp. 62–81. London: Routledge and Kegan Paul Ltd.

YOKOYAMA, T., NAKAI, S. & WAKITA, H. 1999. Helium and carbon isotopic compositions of hot spring gases in the Tibetan Plateau. *Journal of Volcanology and Geothermal Research* **88**, 99–107.

YOSHIMURA, K., LUI, Z., CAO, J., YUAN, D., INOKURA, Y. & NOTO, M. 2004. Deep source CO_2 in natural waters and its role in extensive tufa deposition in the Huanglong Ravines, Sichuan, China. *Chemical Geology* **205**, 141–53.

ZHANG, D. D., ZHANG, Y. & ZHU, A. 2001. Physical mechanisms for river waterfall tufa (travertine) formation. *Journal of Sedimentary Research* **71**, 205–16.